

Stephanie L. Seely¹ and John M. Shuford
ENSCO Inc., Melbourne, FL

1. INTRODUCTION

This presentation is one of three to summarize preliminary work performed jointly by ENSCO Inc. and Battelle Memorial Institute to determine a method for modeling the rate of inactivation of spores of *Bacillus anthracis*, the causative agent of anthrax, under arbitrary environmental conditions. For part II, we describe a method for estimating the rate of inactivation of airborne *B. anthracis* spores by natural sunlight using observed weather data.

Although the analysis of the experimental data in Part I revealed rather significant uncertainty in the results and the need to repeat the experiment with several corrections to the radiometric measurement setup; we are applying those results here simply for the purpose of demonstrating our method.

In Part I, a set of experimental data including UV radiation dosimetry measured by a spectroradiometer and the resulting observed inactivation of aerosolized *B. anthracis* spores was examined. A linear regression relationship was determined between the logarithm of the surviving fraction and biologically effective ultraviolet fluence. That relationship may be expressed as:

$$\frac{N}{N_0} = e^{-kUVt}, \quad (1)$$

where N/N_0 is the fraction of culturable spores remaining after irradiation, UV is total effective irradiance (mW/m^2), t is time (minutes), UVt is effective fluence ($\text{mW min}/\text{m}^2$ at 280 nm), and $-k$ is the slope of the regression line (-0.0105 ($\text{mW min}/\text{m}^2$ at 280 nm)⁻¹).

In order to apply this relationship to a particular environmental scenario, the term UV must be calculated using a radiative transfer model, a biological weighting function (or action spectrum), and the appropriate weather data. Then kUV becomes the new decay constant for an exponential relationship to predict the number of viable spores remaining after time t within that solar radiation environment.

Here we will present some sample calculations of the rate of inactivation and explore the dependence of a predicted rate on environmental variables that affect UVB radiation such as solar zenith angle, ozone column concentration, cloud cover, and elevation.

2. METHOD

We begin by examining some sample spectra (Figure 1). The first ("Summer Solstice") corresponds to

solar noon at 23.5° N latitude on the day of the summer solstice — a harsh UV environment thought to represent the extreme of likely modeling scenarios. This solar irradiance² spectrum was generated using the software package FASTRT, freely available under the terms of the GNU General Public License (Engelsen and Kylling, 1998) (for more details on FASTRT, see the Appendix).

The "midlatitude" spectra are observed solar spectra obtained with permission from van Weele, et al. (2000). They represent two solar zenith angles of 30 and 70 degrees from overhead at a location approximately 47° N latitude during the month of May. The fourth and final spectrum is a representative sample of the UV output by the Xenon lamp at a setting of 700 Watts filtered by a colored glass longpass filter. A setting of 700 Watts was the highest power level that still permitted survival of some spores after a period of 10 minutes.

Note the extreme amounts of UVB ($\lambda < 315$) present in the lamp spectrum, while the UVA output ($\lambda > 315$) by the lamp is approximately similar to that of a solar spectrum very late in the day. In general, solar spectra have proportionally much higher UVB levels when the sun is high in the sky than when the sun is near the horizon (but not in such a large proportion as exhibited by the lamp.) In any case, UVB has greater biological effectiveness in producing kill of the *B. anthracis* spores than UVA. So it is for this reason, as we will show, the rate of loss of viability is more sensitive to zenith angle than to any other environmental variable.

For the next step in calculating a decay rate, we use the Munakata, et al. (1996) action spectrum (normalized by its value at 280 nm) to weight these sample irradiance spectra. The resulting biologically effective irradiance spectra are shown in Figure 2. Total effective irradiance (the area under each curve) describes the relative effectiveness of a particular spectrum for inactivation of the spores.

Table 1 contains the total effective irradiance for each sample spectrum along with a corresponding inactivation rate constant and an equivalent half-life. Figure 3 and Table 2 show survival over time for each case. Note that in the environment, the solar conditions would change over time, so these hypothetical survival curves could be underestimates or overestimates depending

2. Irradiance represents radiant flux, the amount of radiant energy (mJ) which flows through a horizontal unit area (m^2) during a unit time (s) per unit wavelength (nm).

1. Corresponding author address: 445 Pineda Ct.,
Melbourne, FL, 32940. email: seely.stephanie@ensco.com

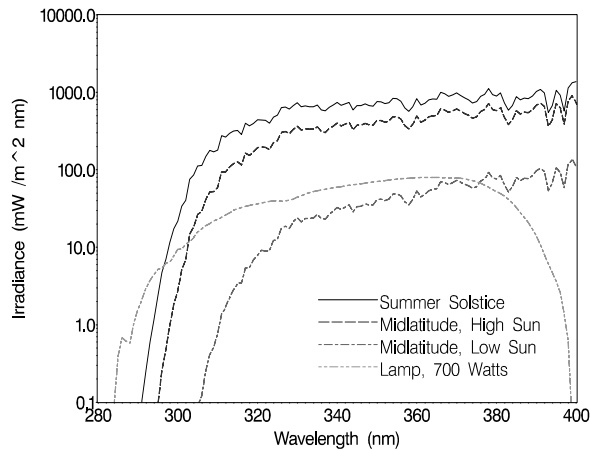


Figure 1. Sample irradiance spectra.

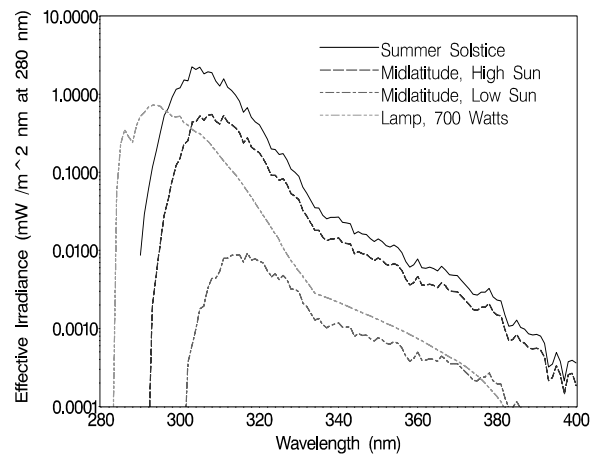


Figure 2. Effective irradiance spectra (sample spectra after biological weighting function is applied).

whether the sun is rising or falling, respectively, during the 400 minutes. For comparison, we have also plotted survival over time according to the conventionally cited rates of 2% per minute¹, a 25 minute half-life, and three loss curves published by the U.S. Army (Figure 4).

3. VARIABILITY

Since the rate of loss of viability is dependent on levels of effective ultraviolet exposure, many variables will influence how long the microorganism retains its viability in the outside environment. The most critical factor in predicting loss of viability is the solar zenith angle. As the sun moves from near the horizon to overhead, the transmission of ultraviolet radiation by the earth's atmosphere increases, and this is especially so for UVB radiation (wavelengths shorter than 315 nm).

1. Two percent (2%) per minute represents a linear recursion coefficient.

Table 1: Rates of loss of viability of the spores under various ultraviolet radiation environments. Effective irradiance is calculated using the Munakata, *et al.* (1996) action spectrum normalized by its value at 280 nm.

Case	I_{eff} (mW/m ² at 280 nm)	k (mW min / m ² at 280 nm) ⁻¹	Half Life (min)
Summer Solstice	34.1	0.36	1.9
Midlatitude, High Sun	9.15	0.096	7.2
Midlatitude, Low Sun	0.184	0.0019	360
Lamp, 700 Watts	6.86	0.072	9.6

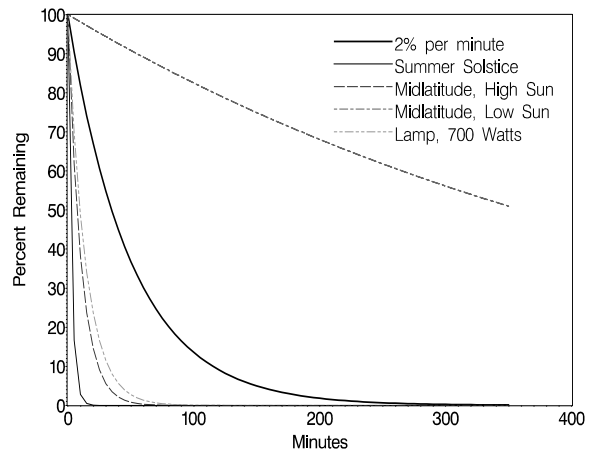


Figure 3. Survival over time under a sample of widely different solar radiation conditions.

Table 2: Tabulated survival over time under a sample of widely differing solar radiation conditions.

Time (min)	Summer Solstice	Midlat, High Sun	Midlat, Low Sun	Lamp, 700 Watts	2% per minute
0	100	100	100	100	100
10	2.8	38.3	98.1	48.7	81.9
20	0.1	14.6	96.2	23.7	67.0
30	0.0	5.6	94.4	11.5	54.9
50	0.0	0.8	90.8	2.7	36.8
100	0.0	0.0	82.5	0.1	13.5
150	0.0	0.0	74.9	0.0	5.0
300	0.0	0.0	56.1	0.0	0.2
500	0.0	0.0	38.2	0.0	0.0

Figure 5 contains a plot of several UV solar spectra at sea level for a progression of solar zenith angles. Observe that the relative proportion of UVB increases (see the curves shift leftward toward the shorter wavelengths) as the position of the sun rises in the sky. Despite the very small amounts of UVB present in sun-

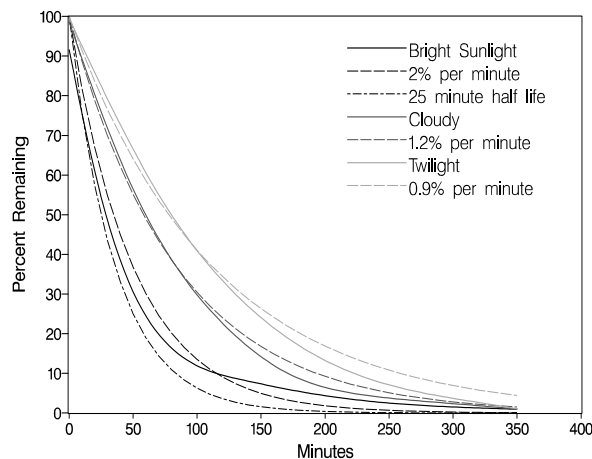


Figure 4. Conventionally cited rates for loss of viability of airborne *B. anthracis* spores. Thick lines are published curves (from *US Army Field Manual FM-3.3*); thin lines were calculated using the exponential rate of inactivation indicated by each published curve, where the half life = $\ln(2.0) / k$. Note the thick curve for bright sunlight falls between the rate of loss implied by “2% per minute” and “25 minute half-life”.

light this radiation is highly effective in producing inactivation of the spores. This can be seen most clearly in the plot in Figure 6 which shows the diurnal variation of biologically effective irradiance. The shortest wavelength bands contain the most effective radiation, and these bands also experience the greatest diurnal variation over the course of the day.

The variation of effective irradiance drives the variation of the inactivation rate constant, shown in Figure 7, where peak inactivation rates are observed at solar noon and the rate of loss declines as the sun approaches the horizon. Note the earlier occurrence of solar noon at the more easternmost location (Bangor, ME), the shorter day, and the consequently earlier sunset.

Second to zenith angle in terms of effect on inactivation rate is the ozone column concentration, since ozone absorbs solar radiation at UVB wavelengths. Higher ozone column concentrations reduce the amount of UVB reaching the earth’s surface, which reduces the rate of spore inactivation. The variation in ozone column concentration at a single location from day to day can be significant: as much as 30 DU for locations in the subtropics, and 80 DU for locations in the upper latitudes.

Other important factors to consider are cloud cover and elevation. Increased cloud cover reduces surface UV through increased scattering. Higher elevations experience higher levels of UV because of the reduced optical depth of the atmosphere overhead.

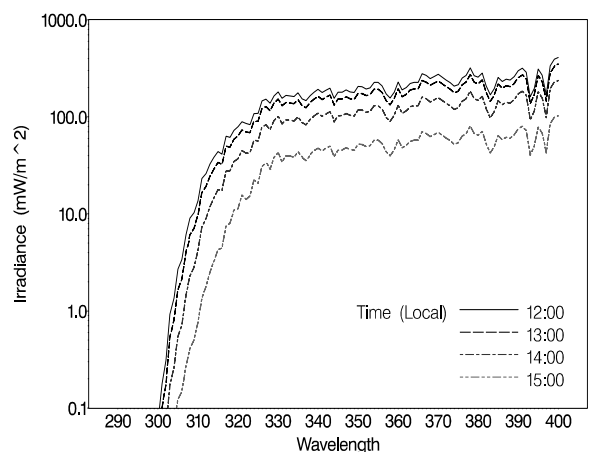


Figure 5. Changes in solar spectral irradiance simulated for a sea level location in the midlatitudes.

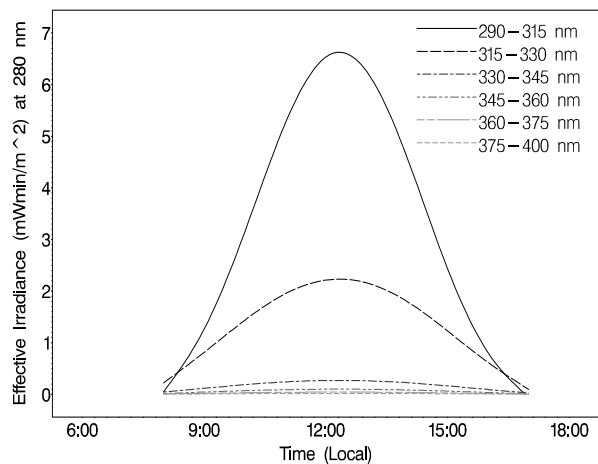


Figure 6. Rise and fall of effective irradiance over a single day for a sea level location in the midlatitudes.

4. MODELING

Among transport models in use today, methods for simulating losses due to decay vary greatly. Many transport models used by the Department of Defense were originally designed to model losses of radioactive material due to radioactive decay, and very few treat biological decay. Those that model radioactive decay usually require a half-life for the species in question, and this remains constant throughout a simulation. That feature makes such a model unsatisfactory for modeling biological decay.

The few models that treat biological decay specifically (SCIPUFF-- Sykes, 1997; and VLSTRACK--Bauer and Gibbs, 1997) require the input of a decay rate from the user, then that rate is adjusted downward to imitate the effect of a falling sun and/or cloud cover. SCIPUFF uses a sinusoidal function of the sun angle to reduce a maximum rate of decay (where the maximum rate is

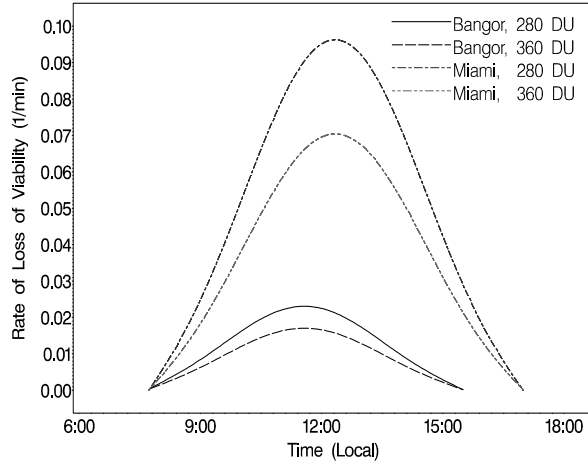


Figure 7. Rise and fall of the predicted inactivation rate for airborne *B. anthracis* spores at two widely separated latitudes for two levels of ozone column concentration.

assumed appropriate for solar noon), and clips the function to go no lower than a minimum nighttime decay rate:

$$k = \max(k_{day} \cdot \sin(\phi), k_{night}). \quad (2)$$

An improved algorithm would automatically select a peak rate for solar noon and calculate the fall-off of that rate as a function of several of the most critical environmental variables. The algorithm we have designed does this through the use of a radiative transfer model, an action spectrum, a preliminary observed correspondence between loss of viability and effective fluence, and observed weather data.

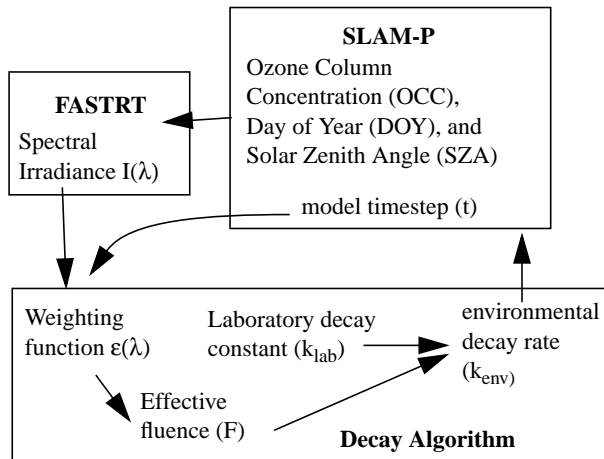


Figure 8. Flow of data between FASTRT, the decay subroutine and the SLAM-P transport and dispersion model.

First, FASTRT is used to generate spectral irradiance as a function of solar angle, ozone column concentration, and day of year. Then effective fluence is calculated using:

$$F_{eff} = \left(\sum_{\lambda=290}^{400} \varepsilon(\lambda)I(\lambda)\Delta\lambda \right) \times \text{model time step} \quad (3)$$

Next, the effective fluence is adjusted for elevation according to Long (1996).

$$adj\left(\frac{\%}{km}\right) = a_0 + a_1 Z_{sfc} + a_2 Z_{sfc}^2 \quad (4)$$

where $a_0 = -0.04556$, $a_1 = 6.62033$, and $a_2 = -0.23067$, and Z_{sfc} is the surface elevation in kilometers above sea level. At 1 km, the adjustment should be an increase of 6.34%. The correction is applied to the effective fluence as $(1.0 + adj/100) \cdot F_{eff}$.

The effective fluence is then reduced by a percentage based on cloud cover at the nearest surface station using cloud attenuation coefficients contained in Table 3 and the relationships in Table 4. The correction is applied to the effective fluence as $CAF \cdot F_{eff}$.

Table 3: Cloud attenuation Factors (http://www.cpc.ncep.noaa.gov/products/stratosphere/uv_index/uv_compute.html, June 14, 2001)

Cloud Condition	Cloud Category (eighths obscured)	Cloud Attenuation Factor (CAF) (%)
Clear	0	1.00
Scattered	2	0.89
Broken	7	0.73
Overcast	8	0.32

Table 4: Regression relationships for calculating CAF.

Cloud Category (eighths obscured)	Relationship
$0 \leq CC \leq 2$	$CAF = -0.055 \cdot CC + 1.0$
$2 < CC \leq 7$	$CAF = -0.032 \cdot CC + 0.954$
$7 < CC \leq 8$	$CAF = -0.41 \cdot CC + 3.6$

There are differences between the rates calculated using the technique we have just described and those obtained using Equation 2 (Figure 9). But clearly, the complexity and interaction of many environmental variables and their effect on the inactivation rate for this microorganism make the use of a radiative transfer model a useful tool for prediction of a decay rate under a given set of environmental conditions.

A summary of the kind of variation produced by this algorithm is tabulated in Table 5 (for decay rate constants) and in Table 6 (for corresponding half-lives).

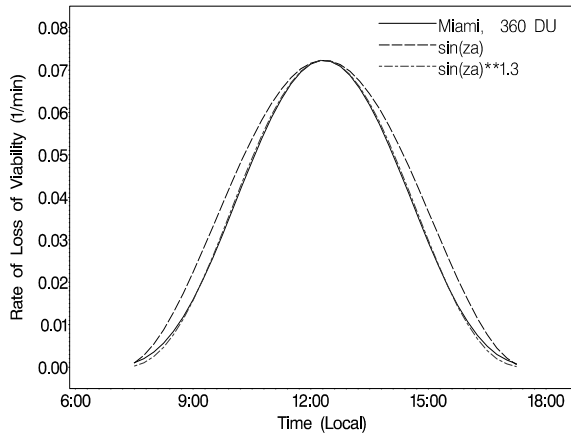


Figure 9. Comparison of three methods for calculating the diurnal variation of the decay rate for UV inactivation of *B. anthracis*.

Table 5: Predicted rate constants for decay (1/min) under a range of environmental conditions. Irradiances were calculated using the radiative transfer model FASTRT, effective irradiance was calculated using the Munakata *et al.* (1996) action spectrum, and both the increase in UV due to rise in elevation and the attenuation of UV due to cloud cover follow NOAA's convention for the same adjustments to the U.S. UV index (Long, 1996).

Cloud Cover (eighths obscured)	Elevation above sea level (km)	Zenith Angle (degrees from overhead)									
		15		25		35		55		85	
		Ozone Column Concentration (Dobson Units)									
		280	450	280	450	280	450	280	450	280	450
Clear	0	2.8E-01	1.5E-01	2.4E-01	1.3E-01	1.8E-01	9.9E-02	7.1E-02	3.9E-02	1.6E-03	9.7E-04
	1	3.0E-01	1.6E-01	2.5E-01	1.4E-01	1.9E-01	1.1E-01	7.5E-02	4.2E-02	1.7E-03	1.0E-03
	5	3.8E-01	2.1E-01	3.2E-01	1.8E-01	2.4E-01	1.3E-01	9.5E-02	5.3E-02	2.2E-03	1.3E-03
5/8	0	3.0E-01	1.6E-01	2.5E-01	1.4E-01	1.9E-01	1.1E-01	7.6E-02	4.2E-02	1.7E-03	1.0E-03
	1	2.5E-01	1.4E-01	2.1E-01	1.2E-01	1.6E-01	9.0E-02	6.4E-02	3.6E-02	1.4E-03	8.8E-04
	5	2.6E-01	1.4E-01	2.2E-01	1.2E-01	1.7E-01	9.1E-02	6.5E-02	3.6E-02	1.5E-03	8.9E-04
Overcast	0	8.2E-02	4.5E-02	6.9E-02	3.8E-02	5.3E-02	2.9E-02	2.1E-02	1.2E-02	4.7E-04	2.8E-04
	1	2.8E-02	1.5E-02	2.4E-02	1.3E-02	1.8E-02	9.9E-03	7.0E-03	3.9E-03	1.6E-04	9.7E-05
	5	1.1E-02	6.2E-03	9.6E-03	5.3E-03	7.3E-03	4.0E-03	2.9E-03	1.6E-03	6.5E-05	3.9E-05

Table 6: (As in Table 5) Corresponding predicted half-life in minutes under a range of environmental conditions.

Cloud Cover (eighths obscured)	Elevation above sea level (km)	Zenith Angle (degrees from overhead)									
		15		25		35		55		85	
		Ozone Column Concentration (Dobson Units)									
		280	450	280	450	280	450	280	450	280	450
Clear	0	2	5	3	5	4	7	10	18	435	716
	1	2	4	3	5	4	7	9	17	409	674
	5	2	3	2	4	3	5	7	13	322	529
5/8	0	2	4	3	5	4	6	9	16	405	666
	1	3	5	3	6	4	8	11	19	480	789
	5	3	5	3	6	4	8	11	19	475	781
Overcast	0	8	15	10	18	13	24	33	60	1483	2440
	1	25	45	29	54	39	70	98	177	4359	7171
	5	61	111	72	131	95	171	242	434	10701	17606

5. SUMMARY

We have summarized a method for predicting the rate of loss of viability of airborne *B. anthracis* spores for any solar radiation environment. That environment may be defined by sun angle, ozone column concentration, elevation above sea level, and cloud cover. The method relies on the use of a radiative transfer model (RTM) for the calculation of solar spectral irradiance.

For implementation within an emergency response transport and dispersion model or a battlefield hazard prediction model, the complexity of the prediction algorithm would depend on the selected RTM and the desired number of RTM inputs. Additional inputs might be visibility, to approximate the attenuating effect of increased aerosol optical depth, and other aerosol parameters such as aerosol angstrom coefficients and vertical profile. Surface albedo also has a significant effect on surface UV irradiance levels. However, until a

more precise estimate of the relationship between the rate of loss of spore viability and effective fluence can be obtained in the laboratory, the increased computational requirement of a full-scale radiative transfer model and extensive input parameters is probably not justified.

6. APPENDIX

FASTRT calculates irradiance by spline interpolation of effective transmittances stored in look-up tables. The RADTRAN atmospheric radiative transfer software package (based on the multi-stream discrete ordinates radiative transfer equation solver DISORT by Stamnes *et al.* (1988)) was used to produce the look-up tables, where computations were performed using the pseudospherical approximation (SDISORT) by Dahlback and Stamnes (1991) in order to ensure high levels of accuracy even for low solar elevations. The settings used by RADTRAN are detailed in the following table.

Table 7: The FASTRT lookup tables were computed using RADTRAN version 0.06 assuming the following atmospheric and surface conditions.

Input Parameter	Setting
Atmosphere	AFGL US standard atmosphere (Anderson <i>et al.</i> , 1986)
Surface albedo	0.02 at all wavelengths
Surface altitude	0.0 kilometers
Extraterrestrial Irradiance	The Solar ultraviolet Spectral Irradiance Monitor (SUSIM) extraterrestrial solar spectrum measured on board the Space Shuttle during the ATLAS 3 mission in November 1994 (Van Hoosier, 1996).
Aerosol angstrom coefficients	$\alpha=1.3$, $\beta=0.02$ where optical depth = $\beta\lambda^{-\alpha}$, and λ is in μm
Visibility	23 km (determines the relative amount of aerosol in the troposphere)
Ozone absorption crosssection	Molina and Molina (1986)
Aerosol profile	spring/summer (Shettle, 1989)
Tropospheric aerosol	rural type (from MODTRAN3)
Stratospheric aerosol	background conditions (from MODTRAN3)
Radiation Transfer equation solver	SDISORT (Dahlback and Stamnes, 1991), i.e., a pseudo-spherical version of DISORT (Stamnes K <i>et al.</i> , 1988)
forward aerosol scattering	Delta-M approximation
Number of Radiative Streams	12
Atmospheric Layers	49

7. REFERENCES

- Anderson, G.P., Clough, S.A., Kneizys, F.X., Chetwynd, J.H., Shettle, E.P. (1986) AFGL Atmospheric constituent profiles (0-120 km). Tech. Rep. AFGL-TR-86-0110, Air Force Geophys. Lab., Hanscom Air Force Base, Mass.
- Bauer, T.J. and Gibbs, R. (1997) Software User's manual for the chemical/biological agent Vapor, Liquid, and Solid Tracking (VLSTRACK) computer model, Version 1.6.3 (windows). NSWCDD/MP-97/196, Naval Surface Warfare Center, Dahlgren, VA, 22448-5100.
- Beebe, J.M. *et al.* August 1962. Stability and Virulence Relationships of Airborne Bacillus Anthracis Spores under Stress of Light and Humidity, (Technical Memorandum No. 18). Aerobiology Division, U.S. Army Biological Laboratories, Frederick, Maryland.
- Dahlback A., and Stamnes, K. (1991) A new spherical model for computing the radiation field available for photolysis and heating at twilight. *Plan. Space Sci.*, 39, 671-683.
- Engelsen, O. and Kylling, A. (1998) "Fast radiation transfer modeling of downward UV doses, indices and irradiances at the Earth's surface", European Conference on Atmospheric UV Radiation, Helsinki, 28 June - 2 July 1998. <http://zardoz.nilu.no/~olaeng/fastrt/fastrt.html>
- Headquarters, Dept. of the Army, 16 November 1992, Chemical and Biological Contamination Avoidance, Field Manual No. 3-3, Washington D.C..
- Long, C.S., Miller, A.J., Lee, H-T., Wild, J.D., Przywarty, R.C., and Hufford, D. (1996) Ultraviolet Index Forecasts Issued by the National Weather Service. Bul-

letin of the American Meteorological Society, 77, 729-748.

Molina and Molina (1986) Journal of Geophysical Research, 91, 14501-14508.

Molina and Molina (1986) Journal of Geophysical Research, 91, 14501-14508.

Munakata, N., Morohoshi, F., Hieda, K., Suzuki, K., Furu-sawa, Y., Shimura, H., and Ito, T. (1996) Experimental correspondence between spore dosimetry and spectral photometry of solar ultraviolet radiation. Photochemistry and Photobiology, 63, 74-78.

Shettle, E.P. (1989) Models of aerosols, clouds and precipitation for atmospheric propagation studies, In "Atmospheric propagation in the UV, visible, IR, and MM-region and related system aspects", AGARD Conf. Proc., pp. 15-1 - 15-13.

Stamnes, K., Tsay, S.C., Wiscombe, W., and Jayaweera, K. (1988) A numerically stable algorithm for discrete ordinate method radiative transfer in multiple scattering and emitting layered media, Applied Optics, 27, 2502-2509.

Sykes, I., et al. (1997) "PC-SCIPUFF Version 1.0 Technical Documentation", Titan Corporation, A.R.A.P Report No. 716.

Van Hoosier (1996) ftp:susim.nrl.navy.mil, cd pub.uars.